Publication P6

Seman, S., Niiranen, J., Arkkio, A. 2006. “Ride-Through Analysis of Doubly Fed Induction Wind-Power Generator under Unsymmetrical Network Disturbance”, *IEEE Transaction on Power Systems*, Accepted for future publication, 7 p.

Ride-Through Analysis of Doubly Fed Induction Wind-Power Generator Under Unsymmetrical Network Disturbance

Slavomir Seman, *Student Member, IEEE*, Jouko Niiranen, *Senior Member, IEEE*, and Antero Arkkio

***Abstract*—This paper presents a ride-through simulation study of a 2-MW wind-power doubly fed induction generator (DFIG) under a short-term unsymmetrical network disturbance. The DFIG is represented by an analytical two-axis model with constant lumped parameters and by a finite element method (FEM)-based model. The model of the DFIG is coupled with the model of the active crowbar protected and direct torque controlled (DTC) frequency converter, the model of the main transformer, and a simple model of the grid. The simulation results show the ride-through capability of the studied doubly fed wind-power generator. The results obtained by means of an analytical model and FEM model are compared in order to reveal the influence of the different modeling approaches on the short-term transient simulation accuracy.**

***Index Terms*—Active crowbar, direct torque control (DTC), doubly fed induction generator (DFIG), modeling, unsymmetrical disturbance, variable speed wind turbine.**

I. Introduction

THE VARIABLE speed wind turbines with doubly fed induction generators (DFIG) are nowadays becoming more widely used in wind power generation. Due to the increase of the number of the wind turbines connected to the grid, new grid codes have been issued that require ride-through capability of the wind-power generation system. Instead of disconnection, the wind generators have to support the network during the power disturbances in the network [1], [2]. Therefore, it is necessary to carry out accurate transient simulations in order to understand the impact of the power system disturbances on a wind turbine operation.

In the recent years, the ride-through analysis of the DFIG wind turbine under network disturbance has become an intensively studied problem. The low-voltage ride-through analysis of the 2-MW Vestas V80VCS wind turbine has been presented in [3]. This paper shows the ability of the ride-through during the 50% voltage dip without using the crowbar. This paper also shows that mechanical model of the wind turbine could be neglected because it affects the transient behavior of DFIG minimally as it has been also stated in [4]. A theoretical ride-through study of the DFIG wind generator under three-phase network fault is presented in [5], where the crowbar is used in order to protect the rotor-side converter and rotor of the generator.

Most of the DFIG wind generators transient studies have been focused on the voltage dip analyses due to symmetrical three-phase network fault [6]–[9]. These kinds of faults, however, are very seldom. Single and two-phase earth faults are more common. Moreover, two-phase faults are more demanding for a DFIG than symmetrical three-phase faults. Thus, more research about unsymmetrical fault ride-through performance is required.

Most DFIG wind turbine models that are used in transient analyses represent the generator by means of a two-axis model with constant lumped parameters [3], [5]–[10]. A model of DFIG that takes into account the equivalent circuit parameter variation was presented in [11].

A significant part of the wind turbine model is the model of a frequency converter that supplies the rotor of the DFIG. As it was stated in [12], the converter is found to be the most sensitive part of the wind turbine when subjected to a short-circuit fault in the grid.

The control of a frequency converter is usually based on field-oriented control as shown in [13], but also, the modified direct torque control (DTC) could be used as presented in [14]. The frequency converters are usually equipped with a rotor overcurrent protection circuit that is commonly called crowbar [15]. The crowbar protects the rotor-side frequency converter against the high rotor current transient that DFIG generates during the disturbance.

This paper presents a ride-through simulation study of a 2-MW wind-power DFIG under a short-term unsymmetrical network disturbance. The mechanical part of the wind turbine is omitted, and reference torque and rotor speed is considered to be constant. The DFIG is represented by an analytical two-axis model with constant lumped parameters and by a finite element method (FEM)-based model [16]. The model of the DFIG is coupled with the model of the active crowbar protected and DTC controlled frequency converter, the model of the main transformer, and a simple model of the grid. The simulation model has been experimentally verified by full-scale measurement setup, as it shown in [17].

The overall structure of the investigated system is depicted in Fig. 1. The simulation results show the ride-through capability of the proposed doubly fed wind-power generator. The results obtained by means of an analytical model and FEM model of

Manuscript received February 16, 2006; revised April 21, 2006. This work was supported in part by the National Technology Agency of Finland, in part by ABB Oy and Fortum Oyj, and in part by the Research Foundation of Helsinki University of Technology. Paper no. TPWRS-00080-2006.

S. Seman and A. Arkkio are with the Laboratory of Electromechanics, Helsinki University of Technology, FIN-02015 HUT, Helsinki, Finland (e-mail: slavomir.seman@hut.fi; antero.arkkio@hut.fi).

J. Niiranen is with ABB Oy, FIN-00381, Helsinki, Finland (e-mail: jouko.niiranen@fi.abb.com).

Digital Object Identifier 10.1109/TPWRS.2006.882471

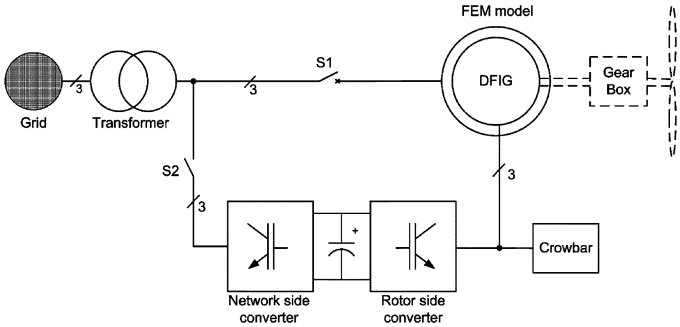

Fig. 1. Overall structure of the DFIG wind turbine.

DFIG are compared in order to reveal the influence of the different modeling approaches on the short-term transient simulation accuracy. The detailed specifications of the DFIG wind generator parameters used in this paper were presented in [17].

II. Method of Modeling

A. Equivalent Circuit-Based Analytical Model of DFIG

The machine equations written in an $x-y$ reference frame fixed with rotor are

$$\frac{d\psi_{s\_x}}{dt} = \sigma_S\left(\frac{L_r}{L_m}\psi_{s\_x} - \psi_{r\_x}\right) - p\omega_r\psi_{s\_y} + v_{s\_x} \quad (1)$$

$$\frac{d\psi_{s\_y}}{dt} = \sigma_S\left(\frac{L_r}{L_m}\psi_{s\_y} - \psi_{r\_y}\right) - p\omega_r\psi_{s\_x} + v_{s\_y} \quad (2)$$

$$\frac{d\psi_{r\_x}}{dt} = \sigma_R\left(\psi_{r\_x} - \frac{L_m}{L_s}\psi_{s\_x}\right) + v_{r\_x} \quad (3)$$

$$\frac{d\psi_{r\_y}}{dt} = \sigma_R\left(\psi_{r\_y} - \frac{L_m}{L_s}\psi_{s\_y}\right) + v_{r\_y} \quad (4)$$

where

$$\sigma_S = \frac{R_s L_m}{L_m L_m - L_s L_r}, \quad \sigma_R = \frac{R_r L_s}{L_m L_m - L_s L_r}$$

$$i_{s\_x} = \frac{L_m}{L_m L_m - L_s L_r}\left(\psi_{r\_x} - \frac{L_r}{L_m}\psi_{s\_x}\right) \quad (5)$$

$$i_{s\_y} = \frac{L_m}{L_m L_m - L_s L_r}\left(\psi_{r\_y} - \frac{L_r}{L_m}\psi_{s\_y}\right) \quad (6)$$

$$i_{r\_x} = \frac{L_s}{L_m L_m - L_s L_r}\left(\frac{L_m}{L_s}\psi_{s\_x} - \psi_{r\_x}\right) \quad (7)$$

$$i_{r\_y} = \frac{L_s}{L_m L_m - L_s L_r}\left(\frac{L_m}{L_s}\psi_{s\_y} - \psi_{r\_y}\right) \quad (8)$$

$$T_e = \frac{3}{2}p(\psi_{s\_y} i_{s\_x} - \psi_{s\_x} i_{s\_y}). \quad (9)$$

The symbols i_s, i_r denote the stator and rotor currents, respectively, v_s, v_r stator and rotor voltages, and ψ_s, ψ_r stator and rotor flux linkages in two axis rotational $(x-y)$ reference frame. R_s, R_r are stator and rotor resistances, and L_s, L_r, L_m are stator, rotor inductances, and magnetizing inductance, respectively. The rotor speed is denoted as ω_r. Symbol p represents the number of pole-pairs, and T_e is the electromagnetic torque. The rotor speed is considered to be a constant, and thus, the equation of motion is omitted as well as the model of the wind turbine mechanical part because the turbine speed behavior has no significant influence on the electrical system performance [3], [4] in case of short-term stability investigations.

TABLE I
Parameters of the DFIG

P_N	rated power	1.7 MW
$U_{N,s}$	rated stator voltage	690 V (delta)
$U_{max,r}$	maximum rotor voltage	2472 (star)
f_N	rated stator frequency	50 Hz
n_N	nominal speed	1500 rpm

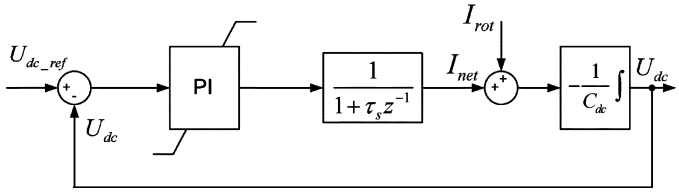

Fig. 2. Simplified model of the network-side converter.

B. Finite Element Model of DFIG

The magnetic field in the generator is modeled by two-dimensional finite element analysis and coupled with the voltage equations of the windings [18].

The FEM computation is implemented as a functional block in Matlab-Simulink using dynamically linked program code (S-function). Voltages of the phase windings in stator and rotor are given as input variables, and the phase currents, electromagnetic torque, rotational speed, rotor position, and flux linkages in stator and rotor are obtained as output variables.

In time-stepping simulation, the FEM computation is coupled with Matlab-Simulink by an indirect procedure [19]. The finite element mesh of the DFIG covers one quarter of the cross section, comprising 949 nodes and 1848 linear triangular elements. The parameters of the DFIG are presented in Table I.

C. Network-Side Converter Model

The network-side converter is represented in simulation by a simplified model, as it is shown in Fig. 2.

The dynamics of the network-side converter are represented in simulator by discrete transfer function, where τ_s denotes the time constant of the first-order discrete filter. The switching dynamics and active and reactive power control are omitted due to the fact that this simplification will not affect significantly the accuracy of the calculated dc-link voltage value [17] that is monitored, and it determines whether or not the crowbar should be activated in the event of the grid fault.

The symbols I_{rot} and I_{net} denote the currents flowing between the dc-link and the rotor-side converter and the dc-link and network-side converter, respectively. The aim of the network-side converter is to supply the dc-link and maintain the level of dc-link voltage U_{dc} on a preset value. U_{dc} is in simulator controlled by PI controller with limiter. The dc-current of the network-side converter I_{net} is limited according to the network voltage magnitude, thus taking into account the ac-current limit of the actual converter.

D. Rotor-Side Converter Model

The rotor-side converter is supplied from a common dc-link, and the switches are assumed to be ideal. The rotor-side frequency converter is controlled by a modified DTC strategy [14].

The magnitude of the rotor flux estimate $|\hat{\psi}_r|$ is obtained as

$$|\hat{\psi}_r| = \sqrt{(\hat{\psi}_{r\_x})^2 + (\hat{\psi}_{r\_y})^2} \tag{10}$$

where symbols $\hat{\psi}_{r\_x}$ and $\hat{\psi}_{r\_y}$ denote the estimated rotor fluxes in the two axis reference frame fixed to the rotor. The rotor flux estimates are

$$\hat{\psi}_{r\_x} = \frac{L_m}{Ls}\hat{\psi}_{sx\_r} + \frac{L_s L_r - L_m^2}{L_s} i_{rx} \tag{11}$$

$$\hat{\psi}_{r\_y} = \frac{L_m}{Ls}\hat{\psi}_{sy\_r} + \frac{L_s L_r - L_m^2}{L_s} i_{ry} \tag{12}$$

where i_{rx}, i_{ry} denote the rotor current components in the two-axis rotational reference frame, and $\hat{\psi}_{sx\_r}$, $\hat{\psi}_{sy\_r}$ denote the x and y components of the stator flux vector estimates in the rotational frame. L_m, L_s, L_r are magnetizing, stator ,and rotor inductances of DFIG, respectively.

The stator flux estimates are obtained by integration of the measured stator voltage after subtraction of the resistive voltage drop of the stator winding. The estimated stator flux is then transformed by a rotator from two-axis stator coordinates to the two-axis rotor coordination system. The magnitude of the grid flux estimate that is used in control for synchronization of DFIG with network is calculated in torque and flux estimator by integrating the measured line-to-line stator voltages transformed into two-axis reference frame. The estimate of electromagnetic torque that is an input of the three-level hysteresis comparator is given by

$$\hat{T}_e = \frac{3}{2} p \frac{L_s L_r - L_m^2}{L_m} (\hat{\psi}_{r\_x}\hat{\psi}_{sy\_r} - \hat{\psi}_{r\_y}\hat{\psi}_{sx\_r}). \tag{13}$$

The reference values of the electromagnetic torque T_{e_ref} as well as rotational speed ω_r are considered to be constant.

The modulus of the desired rotor flux command $|\psi_{r\_ref}|$ obtained from the reference flux calculator as function of the desired reactive power Q_{ref}, given torque command Te_ref, electrical frequency of the DFIG stator side ω_e, and grid flux estimate $|\hat{\psi}_{grid}|$ is given as in (14), shown at the bottom of the page.

The torque and flux hysteresis comparators provide logical output that is used together with the flux sector identification for switching pattern establishment defined by switching state logic. When the switching pattern is established, a voltage vector is applied to the rotor, and this voltage will change the rotor flux. The optimal switching frequency f_{sw} is maintained by means of the hysteresis band control. The block structure of the modified DTC is depicted in Fig. 3.

E. Active Crowbar

The active crowbar is connected between the rotor of DFIG and rotor-side inverter, as it is depicted in Fig. 3. In contrast to the conventional crowbar, the active crowbar is fully controllable.

A typical ride-through sequence [20] starts when the grid voltage decreases rapidly to a low level. This causes high current transients both in the generator stator and rotor. If either the rotor current or dc-link voltage levels exceed their limits, the IGBTs of the rotor-side inverter are blocked, and the active crowbar is turned on.

The crowbar resistor voltage and the dc-link voltage are monitored during the crowbar operation. When these both voltages are low enough, the crowbar is turned off. After a short delay, for the rotor currents decay, the rotor-side inverter is restarted, and the reactive current component of the generator is ramped up in order to support the grid.

Naturally, the crowbar will be turned on again if a too-high rotor current or dc-link voltage is encountered after the turn off of the crowbar. This is often the case with severe two-phase faults that have a high negative-sequence voltage component in the stator. The negative sequence component has a high rotor slip ($s \approx 2$). Thus, very high voltages are induced in the rotor windings that make it impossible to control the rotor current with the available dc-link voltage. Thus, for the most severe unsymmetrical grid faults, the rotor-side inverter cannot be started before the fault has been cleared.

F. Modeling of the Network, Transformer, and Transmission Line

A simple model represents the network with a three-phase voltage source in series with a short-circuit inductance and resistance.

The transmission line between the network and transformer is modeled with its resistance, inductance, and capacitance by a π-equivalent circuit.

The transformer model contains a short-circuit resistance and inductance and stray capacitance of the winding. The transformer is considered to be linear, i.e., magnetic saturation has not been taken into account. A more detailed description of the network, transformer, and transmission line model that has been used in this paper is presented in [17].

III. Simulation Results and Discussion

The simulation analysis was carried out in the Matlab-Simulink system simulator. The system simulator was running

$$|\psi_{r\_ref}| = \sqrt{\left(\frac{(L_s L_r - L_m^2)\, T_{e\_ref}}{L_m |\hat{\psi}_{grid}|}\right)^2 + \left(\frac{L_r}{L_m}|\hat{\psi}_{grid}| + \frac{(L_s L_r - L_m^2)\, Q_{ref}}{\omega_e L_m |\hat{\psi}_{grid}|}\right)^2} \tag{14}$$

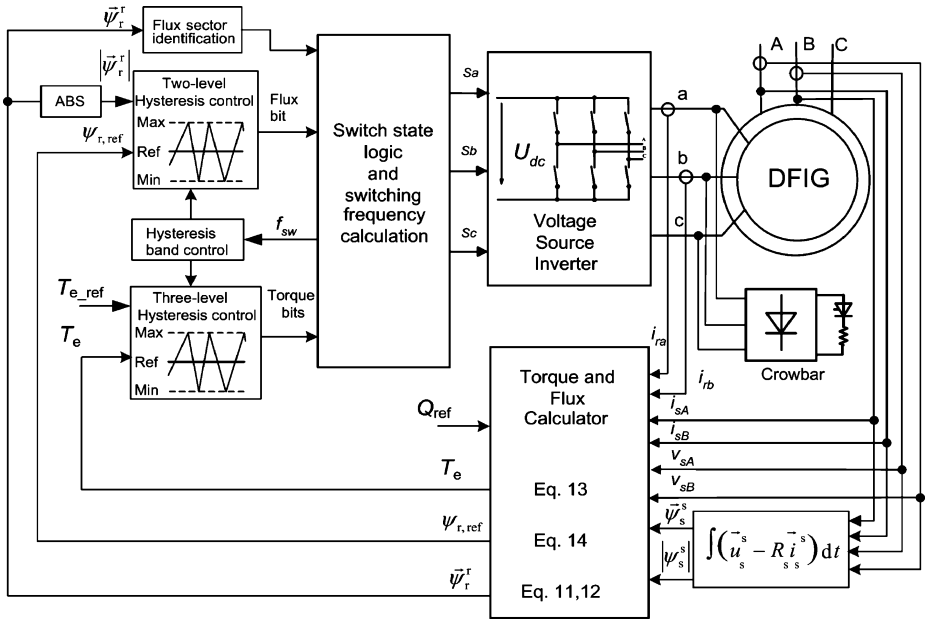

Fig. 3. Block structure of the rotor-side frequency converter controlled by modified DTC with active crowbar.

with the time step $\Delta t = 50$ ns, and the forward Euler method has been used. The simulation results are presented in per-unit system with the base values corresponding to the amplitudes of the respective quantities $V_{\text{base}} = 563$ V, $I_{\text{base}} = 2.03$ kA, and $T_{\text{base}} = 10.9$ kNm. The turns ratio from rotor to stator is $t_r = 3.6$.

A. Synchronization of DFIG and Steady-State Operation

In the first sequence of simulation, the rotor-side converter is started and the DFIG is connected and synchronized with the network. After 2.5 s, the rotor-side converter starts to control the DFIG in torque control mode. The reference torque is set to the required value $Te_{ref} = 0.79$ p.u. at the constant rotor speed $\omega_r = 1.1732$ p.u.

B. Transient Behavior of DFIG During an Unsymmetrical Grid Disturbance

The network disturbance is introduced at time 5 s, when the stator voltages in phases A and C are decreased down to about 56% of the nominal value. The fault is cleared at the time instant 5.7 s, as it is depicted in Fig. 4.

The dc-link voltage in Fig. 5 rises up to 0.6 p.u. at the time instant 5.03 s and exceeds the crowbar triggering limit value. The reason for the dc-link voltage rise in the beginning of the transient is the converters inability to deal with the high inrush current coming from the rotor. The dc-link voltage is decreased and remains stable during the crowbar operation until time instant 5.3 s, when the frequency converter is started again and operates in a reactive power control mode. During this operational mode, the rotor-side converter supports the network with reactive power until time instant 5.7 s, when the fault is cleared and the reference value of the reactive power is set to zero. At the time instance 5.8 s, the rotor-side frequency converter is started to operate in torque control mode.

Fig. 6 depicts the stator currents during the grid disturbance. At the time instant 5.03 s, the high transient current of about 1.75 p.u. is present in phase A and about 1.4 p.u. in phase C. The transient current in phase B that is not under fault is around the rated value. The high currents are reduced in 10 ms by the crowbar down to 0.2 p.u. The frequency converter restarts at time 5.3 s and, after a small transient, starts to operate in a reactive power control mode. The stator current rises up to about 0.8 p.u. until the time instant 5.7 s, when the fault is cleared. The reference reactive power value at the same time instant is set to zero. A 100-ms delay is applied, after which the reference torque is ramped up, and beyond 5.9 s, the amplitude of the stator current corresponds to the demanded torque reference.

Fig. 7 shows the rotor currents during the grid disturbance. A high transient current is present at time 5.03 in phase B with a peak value about 1.7 p.u. and in phase C with a peak value about 2 p.u. The current of a phase A is about 1 p.u. During the crowbar operation, all three currents are kept at low values. The rotor current rises while the frequency converter works in the reactive power control mode after 5.3 s. At time instant 5.7 s, the fault is cleared and the torque is ramped up. The amplitude of the rotor current after 5.9 s is about 1 p.u.

Fig. 8 shows the electromagnetic torque during the grid disturbance. At the time instant 5.03 s, torque rises in the negative direction and its peak value is about -1.3 p.u. During the crowbar operation, the torque is rather smooth with small ripples present.

The amplitude of the torque ripples rises while the frequency converter works in the reactive power control mode after 5.3 s. At the time instant 5.73 s, a quite high ripple is observed due to a transient caused by clearing of the grid fault. At the 5.8 s, the reference torque is ramped up and the electromagnetic torque reaches the demanded value; however, it still oscillates and becomes stabilized after approximately one second.

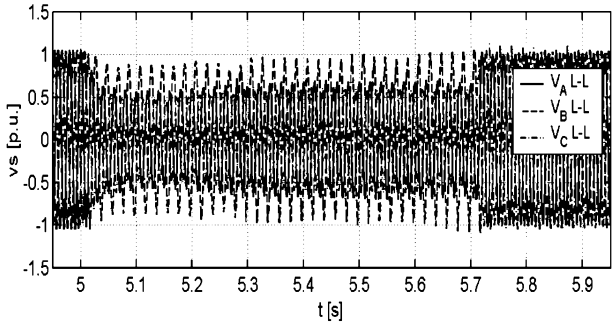

Fig. 4. Stator line-to-line voltage during a grid disturbance.

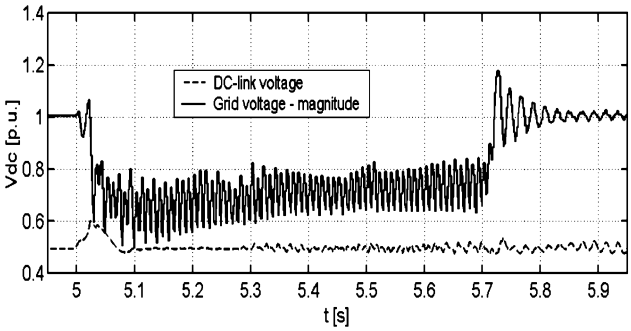

Fig. 5. Dc-link voltage (dash) and filtered grid voltage magnitude (solid) during a grid disturbance.

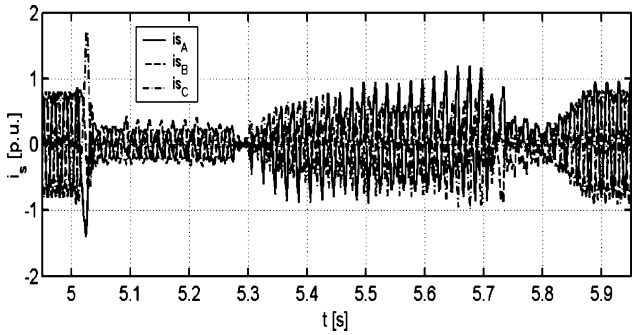

Fig. 6. Stator line current during a grid disturbance.

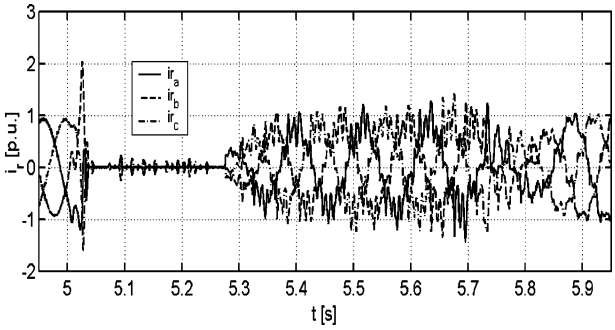

Fig. 7. Rotor line current during a grid disturbance.

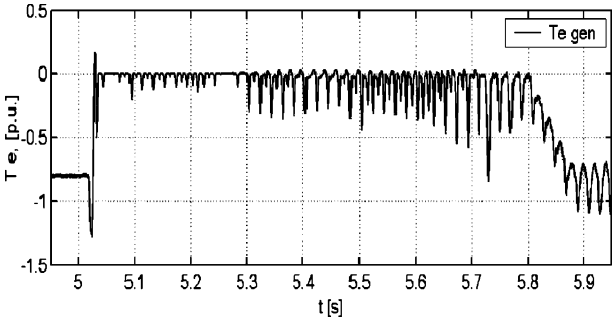

Fig. 8. Electromagnetic torque during grid disturbance.

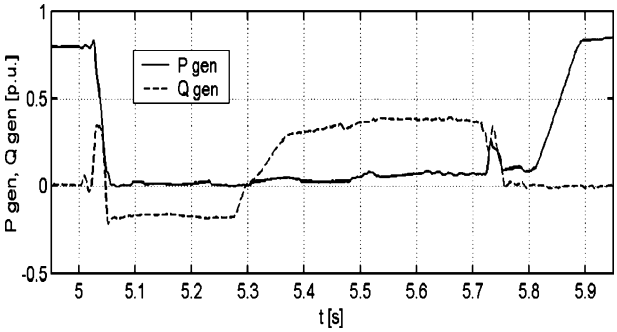

Fig. 9. Active and reactive power of the generator during grid disturbance.

Fig. 9 shows average active power P_{gen} and average reactive power Q_{gen} of the generator, respectively. The average value of the reactive power was calculated by using the 90° delayed voltage method according to

$$P_{gen} = \frac{1}{T}\int_0^T \boldsymbol{u}(t)\boldsymbol{i}(t)dt \tag{15}$$

$$Q_{gen} = \frac{1}{T}\int_0^T \boldsymbol{u}\left(t-\frac{T}{4}\right)\boldsymbol{i}(t)dt. \tag{16}$$

Here, the symbols $\boldsymbol{i}$, $\boldsymbol{u}$ denote the stator phase voltage and line current space vectors, respectively. It is important to note, however, that depending on the used algorithm for the calculation of the average value of the reactive power, the results may differ substantially in case of an unsymmetrical supply. A comparison of several algorithms has been presented in [21]. The future second edition of the IEC 61400-21 standard is expected to define the calculation method used for unsymmetrical dip tests of the wind turbines.

The active power drops rapidly down to zero when the fault is introduced, while the reactive power rises shortly to a value of about 0.35 p.u. At the time instance 5.05 s, after the crowbar is triggered and frequency converter is disconnected, the active power is close to zero, and the reactive power is about −0.2 p.u. Between the time instances 5.05–5.3 s, DFIG behaves as three-phase inductor due to disconnection of the rotor supply and thus consumes reactive power for magnetization. After the time 5.3 s, the frequency converter is restarted and DFIG supports the network with reactive power, demanded value of which is 0.35 p.u. At time instant 5.73 s after the clearance of the fault, the active power rises up for a while but returns to zero, while the reactive power is ramped down to the zero. After a 0.1 s

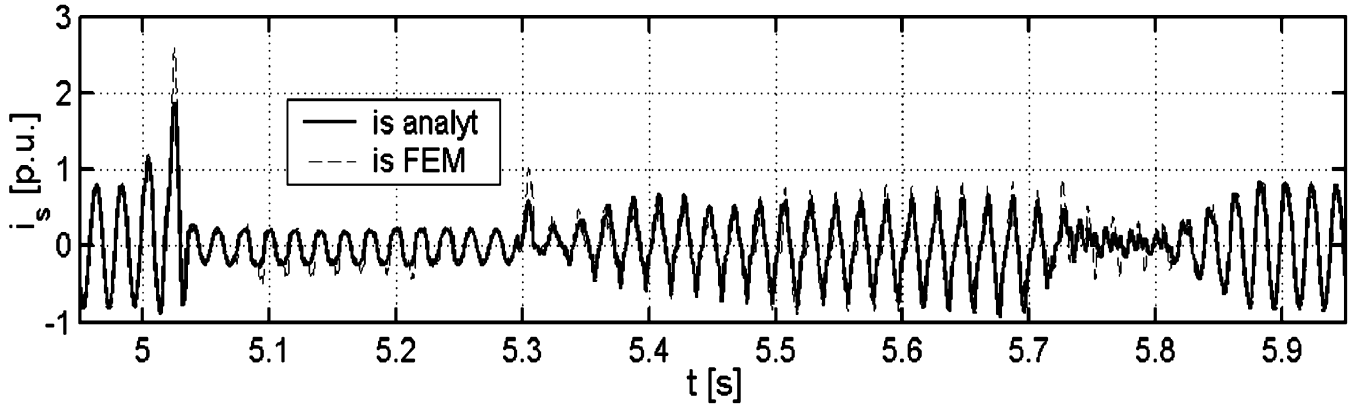

Fig. 10. Comparison of the simulated stator line current obtained by means of the analytical model (solid) and FEM model (dashed).

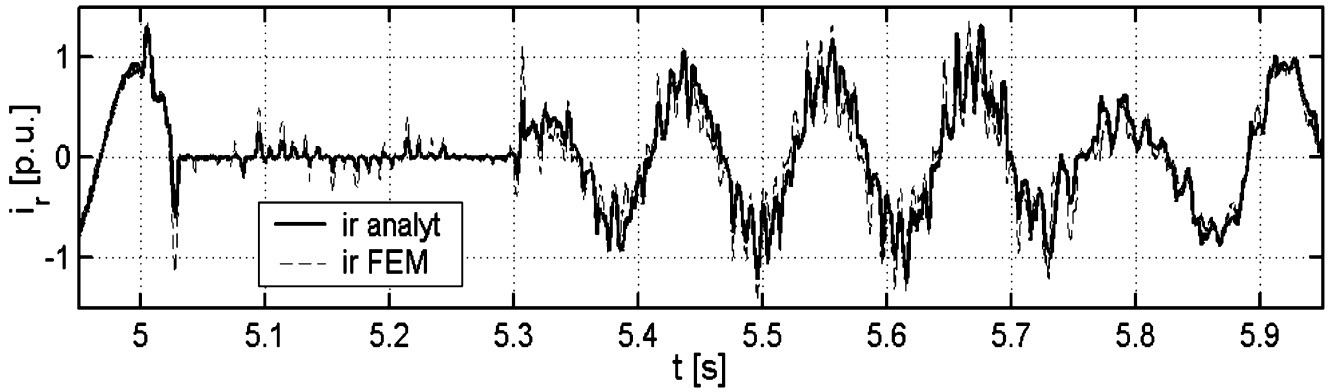

Fig. 11. Comparison of the simulated rotor line current obtained by means of the analytical model (solid) and FEM model (dashed).

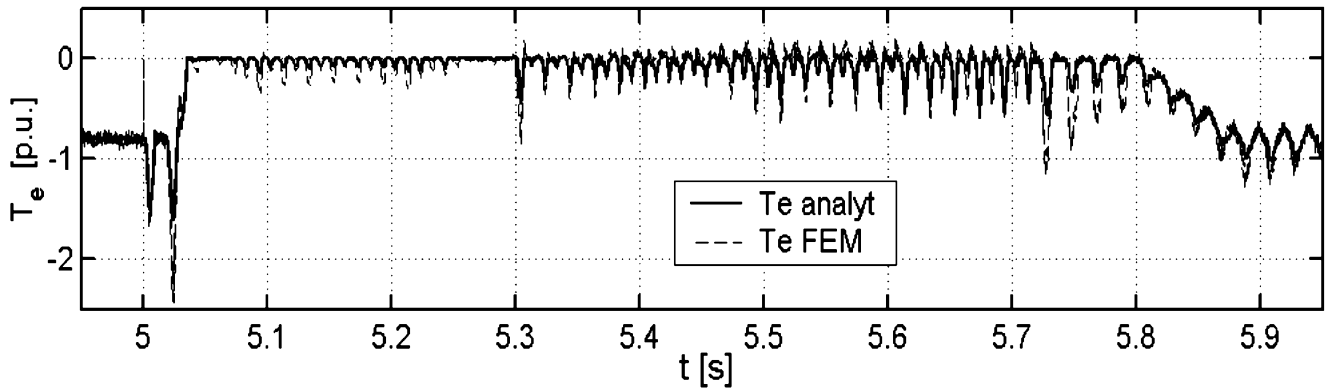

Fig. 12. Comparison of the simulated electromagnetic torque obtained by means of the analytical model (solid) and FEM model (dashed).

delay, the active power is ramped up to the value corresponding to the preset value of the electromagnetic torque, and the reactive power is controlled to be zero.

C. Comparison of the Simulation Results Obtained by the Analytical Model and FEM Model of DFIG

The control part, frequency converter, network, transformer, and crowbar were modeled in Matlab-Simulink, whereas DFIG was modeled by the analytical model and by the time stepping FEM solver. The system simulator (Simulink) was running with a time step $\Delta t = 50$ ns, and the forward Euler method was used. The FEM model of DFIG was running with a time step $\Delta t_{FEM} = 50$ μs.

The stator transient line currents of phase C obtained from the analytical model and FEM model are depicted in Fig. 10. The comparison shows that the FEM current is higher than the analytical one in the first peak at the time instant 5.03 s, and the difference is about 0.7 p.u. After the crowbar is triggered, the stator current is decreased, and during the crowbar operation, both the waveforms show only a small difference. A comparison of the transient rotor currents is depicted in Fig. 11. The amplitude of the rotor current calculated by FEM is in the beginning of the transient higher than the transient rotor current calculated by the

analytical model, and the difference is about 0.5 p.u. A minor difference in amplitude is present during the crowbar operation. Similarly as in the case of the stator current beyond the time instant of 5.3 s, when the converter is started, the FEM current is almost twice the current calculated by the analytical model. A significant difference between the FEM and analytical calculated the rotor current amplitudes can be observed at 5.75 s. The current calculated by FEM is higher, and the difference is about 0.35 p.u.

The more significant difference in the amplitude of the transient stator and rotor currents is present only during the transients when the fault is introduced; the rotor-side frequency converter restarted, and faults cleared. This could be explained so that the FEM model takes into account the magnetic saturation of the stator and rotor leakage inductances.

Fig. 12 depicts the comparison of the generator electromagnetic torque calculated by the FEM model and by the analytical model. The amplitude of the FEM torque is higher than the amplitude of the torque obtained from the analytical model in the beginning of the transient. The difference is about 1 p.u. The difference is small during the crowbar operation. The difference at the time instant 5.3 s is about 0.4 p.u., and after the fault clearance between 5.7–5.76 s, the FEM torque is higher and the difference is about 0.6 p.u.

The large difference in the amplitudes in the beginning of the transient can be explained so that during the unsymmetrical fault the FEM model represents better the unsymmetrical magnetic saturation, while the conventional analytical model neglects all asymmetries. The small differences during the crowbar operation and during the reactive power control mode could be caused also by the different methodology of the electromagnetic torque calculation [17].

IV. Conclusions

The simulation results presented in this paper show one example case of the ride-through operation of the studied doubly fed wind-power generator. The results obtained by means of an analytical model and FEM model of DFIG were compared in order to reveal the influence of the different modeling approaches on the short-term transient simulation accuracy.

The significant difference in the amplitudes of the transient stator and rotor current calculated by FEM and the analytical model of the DFIG have been found, especially when the grid fault has been introduced. Some differences between compared results have also been observed when the rotor-side frequency converter is restarted and when the fault is cleared. This could be explained so that FEM model takes into account the magnetic saturation of the stator and rotor leakage inductances.

The large difference in the compared electromagnetic torque amplitudes in the beginning of the transient could be explained so that during an unsymmetrical fault, the FEM model represents better unsymmetrical magnetic saturation than the conventional analytical model.

The developed coupled field-circuit-based simulator has proved to be capable of complicated power electronics and electric machine setups modeling, and thus, it is a useful tool for the development and optimization of the wind-power generators.

References

[1] E. ON., Netzanschlussregeln Hoch-und Höchstspannung, 2003.

[2] Eltra, Specifications for Connecting Wind Farms to the Transmission Network, ELT 1999-411a, 2004. [Online]. Available: http://www.eltra.dk.

[3] M. Hogdahl and J. G. Nielsen, "Modeling of the Vestas V80 VCS wind turbine with low voltage ride-through," in *Proc. 5th Int. Workshop Large-Scale Integration Wind Power Transmission Networks Offshore Wind Farms*, Glasgow, U.K., Apr. 7–8, 2005, pp. 292–304.

[4] S. Seman, F. Iov, J. Niiranen, and A. Arkkio, "Advanced modeling of doubly fed induction generator wind turbine under network disturbance," in *Proc. 5th Int. Workshop Large-Scale Integration Wind Power Transmission Networks Offshore Wind Farms*, Glasgow, U.K., Apr. 7–8, 2005, pp. 305–314.

[5] J. Morren and S. W. H. de Haan, "Ridethrough of wind turbines with doubly-fed induction generator during a voltage dip," *IEEE Trans. Energy Convers.*, vol. 20, no. 2, pp. 435–441, Jun. 2005.

[6] J. B. Ekanayake, L. Holdsworth, X. G. Wu, and N. Jenkins, "Dynamic modeling of doubly fed induction generator wind turbines," *IEEE Trans. Power Syst.*, vol. 18, no. 2, pp. 803–809, May 2003.

[7] J. G. Slootweg, H. Polinder, and W. L. Kling, "Dynamic modeling of a wind turbine with doubly fed induction generator," in *Proc. IEEE Power Eng. Soc. Summer Meeting*, 2001, vol. 1, pp. 644–649.

[8] L. Holdsworth, X. G. Wu, J. B. Ekanayake, and N. Jenkins, "Comparison of fixed speed and doubly-fed induction wind turbines during power system disturbances," *Proc. Inst. Elect. Eng., Gen., Transm., Distrib.*, vol. 150, no. 3, pp. 343–352, May 13, 2003.

[9] A. Tapia, G. Tapia, J. X. Ostolaza, and J. R. Saenz, "Modeling and control of a wind turbine driven doubly fed induction generator," *IEEE Trans. Energy Convers.*, vol. 18, no. 2, pp. 194–204, Jun. 2003.

[10] T. Petru and T. Thiringer, "Modeling of wind turbines for power system studies," *IEEE Trans. Power Syst.*, vol. 17, no. 4, pp. 1132–1139, Nov. 2002.

[11] S. Seman, S. Kanerva, J. Niiranen, and A. Arkkio, "Transient analysis of wind power doubly fed induction generator using coupled field circuit model," presented at the Int. Conf. ICEM, Cracow, Poland, 2004, unpublished.

[12] V. Akhmatov, "Modelling of variable-speed wind turbines with doubly-fed induction generators in short term stability investigations," presented at the Int. Workshop Transmission Networks Offshore Wind Farms, Stockholm, Sweden, Apr. 11–12, 2002, unpublished.

[13] S. R. Pena, J. C. Clare, and G. M. Asher, "Doubly fed induction generator using back-to-back PWM converters and its application to variable-speed wind-energy generation," *Proc. Inst. Elect. Eng., Elect. Power Appl.*, vol. 143, no. 3, pp. 231–241, May 1996.

[14] K. P. Gokhale, D. W. Krakker, and S. J. Heikkilä, "Controller for a Wound Rotor Slip Ring Induction Machine," U.S. Patent 6741059, May 25, 2004. [Online]. Available: http://www.patft.uspto.gov.

[15] J. Niiranen, "Voltage dip ride through of doubly-fed generator equipped with active crowbar," presented at the Nordic Wind Power Conf., Göteborg, Sweden, Mar. 1–2, 2004 [Online]. Available: http://www.elteknik.chalmers.se/Publikationer/EMKE.publ/NWPCO4/papers/NIRRANEN.pdf, Chalmers Univ. Technol.

[16] S. Kanerva, S. Seman, and A. Arkkio, "Inductance model for coupling finite element analysis with circuit simulation," *IEEE Trans. Magn.*, vol. 41, no. 5, pp. 1620–1623, May 2005.

[17] S. Seman, J. Niiranen, S. Kanerva, A. Arkkio, and J. Saitz, "Performance study of doubly fed wind-power generator under network disturbances," *IEEE Trans. Energy Convers.* [Online]. Available: http://www.ieeexplore.ieee.org/iel5/60/26781/101109TEC2005853741.pdf?tp=&arnumber=101109TEC2005853741&isnumber=26781, to be published

[18] A. Arkkio, "Analysis of induction motors based on the numerical solution of the magnetic field and circuit equations," D.Sc. dissertation, Helsinki, Finland, 1987 [Online]. Available: http://www.lib.hut.fi/Diss/198X/ isbn951226076X/, Acta Polytechnica Scandinavica Electr. Eng. Ser., No. 59.

[19] S. Kanerva, S. Seman, and A. Arkkio, "Simulation of electric drive systems with coupled finite element analysis and system simulator," presented at the 10th Eur. Conf. Power Electronics Applications, Toulouse, France, Sep. 2003. [Online]. Available: http://www.epe-association.org/epe/documents.detail.php?documents_id=441.

[20] R. Virtanen, "Configuration and Method for Protecting Converter Means" International patent application WO2004/091085, Oct. 21, 2004. [Online]. Available: http://www.ofi.epoline.org/view/GetDossier?dosnum=WO2004091085&pubnum=&lang=EN.

[21] *IEEE Standard Definitions for the Measurement of Electric Power Quantities Under Sinusoidal, Nonsinusoidal, Balanced, or Unbalanced Condition (Standard Style)*, IEEE Std. 1459, 2000.

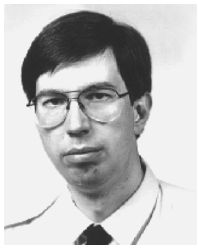

Jouko Niiranen (M'88–SM'03) was born in 1953 in Finland. He received the M.Sc. and Dr. Tech. degrees in electrical engineering degree from Helsinki University of Technology, Helsinki, Finland, in 1980 and 1990, respectively.

Currently, he is a Senior Scientist with ABB Oy, Drives, Helsinki. He started with Stromberg (later ABB) Traction Drives in 1981. From 1989 to 1993, he was as a Researcher with the Power Electronics and Electric Drives Laboratory, Helsinki University of Technology. Since 1993, he has worked with ABB in various research positions. He has also been an Adjunct Professor at Helsinki University of Technology since 1994. His main areas of research interest are modeling and simulation of electric machines, control of high-performance drives, and power electronic converters.

Slavomir Seman (S'03) was born in Presov, Slovakia, in 1973. He received the M.Sc. degree in electrical engineering from the University of Zilina, Zilina, Slovakia, in 1997. He is currently pursuing the D.Sc. (Tech) degree on transient performance study of wind-power generators at Helsinki University of Technology, Helsinki, Finland.

He is a Research Scientist at Helsinki University of Technology. His research interests include numerical analysis of electric machines, modeling and simulation of electric machines, and control of electric drives and frequency converters.

Antero Arkkio was born in Vehkalahti, Finland, in 1955. He received the M.Sc. (Tech) and D.Sc. (Tech) degrees from Helsinki University of Technology (HUT), Helsinki, Finland, in 1980 and 1988, respectively.

He has worked with various research projects dealing with modeling, design, and measurement of electrical machines. He has been a Professor of electrical engineering (electromechanics) at HUT since 2001. Before his appointment as a Professor, he was a Senior Research Scientist and Laboratory Manager at HUT.